Atmospheric Environment During Maneuvering Descent from Martian Orbit

Michael E. Tauber* and Jeffrey V. Bowles†
NASA Ames Research Center, Moffett Field, California
and
Lily Yang‡
Sterling Software, Palo Alto, California

Atmospheric entries from highly elliptical Martian orbits at a speed of 5 km/s are much more difficult than entries from a low-altitude, lower-speed orbit of 3.5 km/s. The higher-speed entries have much more stringent guidance requirements. (The acceptable range of entry flight path angle is less than 0.5 deg, if heating rates are limited so that the vehicle's surface can be radiatively cooled.) In contrast, the lower-speed entries permit variations in flight-path angle of more than 3 deg. A maximum lift/drag ratio of 2.3 was used for all trajectory calculations. The maximum achievable lateral ranges varied from about 3400–2500 km for entry velocities of 5 km/s and 3.5 km/s, respectively, thus permitting a wide choice of landing sites. However, the peak decelerations were an order of magnitude higher for the 5-km/s entries than for the 3.5-km/s entries. Efforts to reduce the deceleration for the higher-speed entry by lift modulation achieved a 40% reduction, but at the expense of decreasing the lateral range by 50%. The vehicle entering at 3.5 km/s along a gliding trajectory encountered a much more benign atmospheric environment. The heat loads for both entry speed were comparable, since the glider experienced a longer heating pulse. However, the glider's peak equilibrium wall temperatures were about 700 K lower. Also, the glider's peak deceleration was only about 0.7 Earth g, making the shallow flight path ideal for manned vehicles whose crews might have been physically weakened during the long voyage to Mars.

Nomenclature

A = reference area of entry vehicle
a = acceleration
C_D = drag coefficient
C_L = lift coefficient
D = drag
g = acceleration of gravity
g_w = ratio of wall enthalpy to total enthalpy
L = lift
l = lateral distance
m = vehicle mass
$\dot{q}$ = heat-transfer rate into the body per unit area (W/cm^2)
R_o = planetary radius
r_n = body nose radius, m
s = distance along trajectory
T_w = equilibrium wall temperature
t = time
V = flight velocity, m/s
V_f = final velocity at end of turn
V_i = initial velocity at beginning of turn
V_s = surface grazing (circular) satellite speed
Y = side force
α = angle of attack
γ = flight-path angle
β = inverse atmospheric density scale height
ψ = turn angle
ρ = freestream density, kg/m^3
ρ_i = reference value of atmospheric density
ϕ = bank or roll angle, measured from horizontal

Subscripts
E = entry condition
o = stagnation point

Introduction

FOR the vehicle designed to land humans on Mars' surface, or to collect soil samples for return to Earth, a suitable landing site may be very important. Since a low lift-to-drag (L/D) vehicle is constrained to land within a hundred kilometers or so of the plane of the orbit from which the vehicle entered the atmosphere, the choice of landing sites would be severely limited. The choice of landing sites can be increased and mission flexibility enhanced by using high L/D vehicles, which have large longitudinal and lateral ranges. For example, a vehicle with a peak L/D ratio of 2.3 would have a lateral range of 2500 km, or greater, making even the remote Martian polar regions accessible. Since the northern polar cap consists primarily of water ice, samples from the ice cap's edge may reveal indications of past biological activity. Lift can also be used to alleviate the deceleration loads and aerodynamic heating accompanying the atmospheric entries, resulting in lower structural and thermal protection weights.

The present paper contains an analysis of the atmospheric maneuvering capability of, and the entry environment encountered by, a vehicle designated to land on the Martian surface. A relatively small vehicle about 10 m long, suitable for the sample return mission, was assumed. However, the overall conclusions of the study should also be applicable to a larger manned vehicle. Presented first is the hypersonic aerodynamic analysis of a proposed high L/D configuration. Next, parabolic (5 km/s) and circular (3.5 km/s) entry velocity trajectories are studied, with emphasis on achieving long lateral ranges and/or modest deceleration. Lastly, the atmospheric heating encountered along the trajectories will be discussed.

Presented in part as Paper 88-2671 at the AIAA Thermophysics, Plasmadynamics, and Laser Conference, San Antonio, TX, June 27–29, 1988; and in part as Paper 88-4345 at the AIAA Flight Mechanics Conference, Minneapolis, MN, Aug. 15–17, 1988; received Sept. 8, 1988; revision received Feb. 27, 1989.

*Research Scientist. Associate Fellow AIAA.
†Research Scientist.
‡Professional Staff Member.

Table 1 Atmospheric density profile constants

Altitude range, km	ρ_i, kg/m^3	β_i, m^{-1}
>36	0.03933	0.1181 (10^{-3})
9 to 36	0.01901	0.09804 (10^{-3})
<9	0.01501	0.07124 (10^{-3})

Analysis

The composition and structure of the atmosphere were determined from measurements made by two U.S. Viking spacecraft that landed on Mars in 1976. Onboard instruments measured each vehicle's deceleration and the atmospheric properties during descent. Additional data were taken after landing. From a combination of these measurements, the atmospheric composition was found to be 95.7% CO_2, 2.7% N_2, and 1.6% A. In addition, altitude variations of temperature, pressure, and density were determined.[1] For entry trajectory calculations, the variation of density with altitude is of primary importance. The data from Ref. 1 were fitted with a series of three exponential expressions of the form

$$\rho = \rho_i e^{-\beta_i y} \tag{1}$$

to define the density at altitudes below 90 km, where atmospheric forces and heating become significant. The values used for the constants ρ_i and β_i are listed in Table 1.

The analysis begins with a brief description of the hypersonic aerodynamic methods that are used to estimate the aerodynamic performance of the proposed vehicle in the Martian atmosphere. Next the formulation of the trajectory equations is presented. The analysis concludes with a discussion of the atmospheric deceleration and heating relationships.

Aerodynamics

Achieving a large lateral range is of primary importance to the present mission. Therefore, a vehicle having a high L/D is required since the lateral range is proportional to the square of the L/D, to first order.[2] For the present mission, a maximum L/D of 2, or greater, is desirable. For example, the Shuttle Orbiter's peak L/D is slightly under 2.[3] By necessity, winged configurations must be used to achieve the desired L/D. A delta-winged vehicle with a leading-edge sweepback of 70 deg is postulated here. To limit the heating rates, however, the wing leading edge must be blunted, as must the nose. The blunt nose and wing leading edge account for a large fraction of the vehicle's drag at hypersonic speeds. The choice of nose and leading-edge bluntness, therefore, must represent a compromise between the aerodynamic need for low drag and the requirement to limit the heating rates.

The calculation of the vehicle aerodynamic characteristics began with the determination of the vehicle's external mold-line geometry definition. Starting with a preliminary configuration layout sketch, a generalized aircraft graphics system was used to generate a numerical model of the external surface, including fuselage, wing, and vertical tails.[4] Using a family of cylindrical sections coupled to the gross geometric parameters, such as sweep and taper ratio, a series of panels and their intersections were computed, which defined the area and unit normal for each panel on the vehicle. The panel sections were then used in the aerodynamic estimating routines to compute high-speed lift and drag characteristics.

The high-speed aerodynamics of the vehicle were calculated using a combination of Newtonian flow theory for lift and pressure drag coupled to a boundary-layer model for estimation of skin-friction drag. The lift and pressure drag were computed by integrating the Newtonian theory pressures over the surface of the vehicle, and resolving the net force in the lift and drag directions. The pressure coefficient was calculated as a function of the local surface incidence, assuming that the specific heat ratio was unity. This assumption is more valid in a predominantly CO_2 atmosphere than in air. At the blunt nose and along the wing leading edge, which contribute most of the pressure drag, the specific heat ratio is about 1.1 and 1.15, respectively,[5] at high speeds.

The friction drag was computed using the Eckert reference enthalpy method.[6] The thermodynamic and transport properties of CO_2 were taken from Ref. 5 and Ref. 7, respectively. Local boundary-layer edge velocity, temperature, and pressure were computed on the body and wing using shock-expansion theory along a streamwise cut assuming an equilibrium, real gas, Prandtl–Meyer flow. Flow properties along the leading edge were computed for a detached bow shock. Newtonian theory was used to calculate the pressures as a function of the angular displacement from the leading-edge stagnation line. The starting point for the Prandtl–Meyer expansion flow was found when the local Mach number exceeded unity. Boundary-layer transition was modeled by using a correlation of local Mach number and edge Reynolds number based on momentum thickness. The transitional boundary-layer length was assumed to be equal to the preceding laminar boundary-layer run. In the transition zone, linear interpolation with distance between laminar and turbulent skin-friction coefficients was used. Base drag was computed assuming a variation in base pressure coefficient equal to the inverse of the freestream Mach number squared, and as a function of base area to reference area ratio. Overall vehicle drag levels were then computed by combining the vehicle component drag contributions with estimated interference and protuberance values from Ref. 8.

Trajectories

The differential equations of motion constituting the trajectory relations for a nonrotating planet[9] were solved numerically. Atmospheric entry was defined to occur at an altitude of 90 km above the Martian surface. The entry velocities are varied from the Martian parabolic speed of 5 km/s to the circular value of 3.5 km/s corresponding to entry from a low planetary orbit. Since the ability to maneuver during descent is of primary importance, the maximum lateral range case requiring a 90-deg heading change is also investigated at both entry velocities. The supercircular speed, 5 km/s, entry trajectories will have large altitude fluctuations, or skipping motions if the maximum lateral range is to be achieved. The amplitude of the skips will be especially pronounced since the entries must be made at shallow angles to limit heating rates and deceleration loads.[2] It will also be shown that when the amplitude of the skips is reduced for parabolic speed entries, the lateral range is severely shortened. However, the circular speed, 3.5 km/s, entries should be nearly smooth, very shallow, glide paths.

A turn, or change of heading, can be performed when a side force, Y acts on the vehicle. The side force acts normal to the lift and drag, and is given by

$$Y = mV^2 \frac{d\psi}{ds} \tag{2}$$

where ψ is the lateral angle through which the trajectory has been turned from its initial direction. The side force results from rotating the lift force by banking the vehicle through an angle ϕ and is

$$Y = L \sin\phi \tag{3}$$

Simultaneously, the lift is reduced by $\cos\phi$.

The general expression for the incremental change in turning angle is

$$d\psi = -\frac{L \sin\phi \, dV}{(D + mg \sin\gamma)V \cos\gamma} \tag{4a}$$

where the relation $V\cos\gamma = \mathrm{d}s/\mathrm{d}t$ has been used. For shallow gliding flight, $\gamma \ll 1$, and Eq. (4a) reduces to[2]

$$\mathrm{d}\psi = -\frac{L}{D}\sin\phi\frac{\mathrm{d}V}{V} \tag{4b}$$

The incremental lateral distance covered during the heading change is

$$\mathrm{d}l = \sin\psi\ \mathrm{d}s \tag{5}$$

Therefore, the lateral distance covered during the turn becomes

$$l_1 = \int_{t_i}^{t_f}\left(\sin\int_{V_i}^{V_f}\mathrm{d}\psi\right)V\cos\gamma\ \mathrm{d}t \tag{6}$$

where the lower and upper limits of integration are the times and velocities at which the turn is begun and completed, respectively. The lateral range consists of the sum of l_1 and the residual range in the direction that the vehicle is heading after completing the turn, and is[2]

$$l = l_1 - \frac{R_o}{2}\frac{L}{D}\ell n\left[1-\left(\frac{V_f}{V_s}\right)^2\right] \tag{7}$$

The bank angle is determined so as to maximize the altitude at the conclusion of a gliding turn[10]; numerical values are also shown in Ref. 10. For the trajectories considered, the bank angles from Ref. 10 are used as starting values and then varied to achieve the maximum lateral range.

Since the lift is reduced during lateral maneuvers, the vehicle descends more quickly than in longitudinal flight. Therefore, a constraint specifying a minimum pullout altitude of 13 km was imposed to prevent the vehicle from colliding with all but the tallest mountains. The altitude constraint requires limiting the vehicle's descent rate in the thin Martian atmosphere; the limit determines the maximum wing loading. The faster descent rates that occur during maneuvers also increase the vehicle's deceleration and heating rates. The total deceleration experienced by the vehicle is given by[2]

$$a = \frac{\mathrm{d}V}{\mathrm{d}t}\left[1+\left(\frac{L}{D}\right)^2\right]^{1/2} \tag{8}$$

where $\mathrm{d}V/\mathrm{d}t$ is the deceleration component tangential to the flight path.

Heating

The Martian atmospheric-entry velocities considered here are modest in comparison with the entry speed of the Space Shuttle Orbiter; however, the heating rates can exceed those experienced by the Shuttle. Since the proposed vehicle is much smaller than the Shuttle, the nose and leading-edge radii must be correspondingly smaller to achieve similar, or better, aerodynamic performance. Therefore, the critical nose and wing leading-edge regions can experience more severe heating than those on the Shuttle. Although a major advantage of a winged vehicle is the ability to make gliding entries (at circular speed) so that heating rates are modest, the duration of the heating pulse can be long. Therefore, extensive insulation is required to protect the vehicle's structure. Despite the insulation requirements, passive thermal-protection systems are desirable. Passive systems are more reliable and are usually lighter than active systems. Although ablation can be very efficient when heating rates are high, it has the disadvantage of producing a rough surface. At the nose, where the boundary layer is thin, the roughness can trigger early transition to turbulence, thus increasing heating and drag. In addition, most ablators still require significant amounts of backface insulation. In contrast, lifting entry at the 5-km/s parabolic speed results in a skipping flight path of shorter duration, but with much more severe heating rates occurring near the bottom of each skip.[2]

The heating will be evaluated at the vehicle's stagnation point and at the wing leading edge. Initially, both convective and radiative heating were considered, since the CO and CN molecules are known to be intense radiators.[11] However, because the highest stagnation-point equilibrium shock layer temperature does not exceed 3300 K and because of the low concentration of nitrogen in the atmosphere, the radiative heating was found to be negligibly small compared with the convective heating. The convective stagnation-point heating will be calculated by using the correlation shown in Ref. 12, which gives (in Watts per square centimeter)

$$q_o = 1.35(10^{-8})\left(\frac{\rho}{r_n}\right)^{1/2}V^{3.04}(1-g_w) \tag{9}$$

A comparison of Eq. (9) with shock tube and ballistic range data[13] shows good agreement (see Fig. 1). It is noteworthy that the stagnation-point convective heating rates in CO_2 are only slightly higher than the rates in air over the velocity range of interest here.

The stagnation-point heating relation given by Eq. (9) is based on the assumption that the wall is fully catalytic. Finite-rate wall catalysis effects were estimated based on calculations made for several flight conditions by our colleague, Paul Kolodziej, for representative surface reactivities in a pure CO_2 planetary atmosphere. By assuming that the surface catalicity was proportional to the mass-fraction of atoms, a correlation was derived which was applicable over a broad range of flight conditions. Based on this assumption, an estimated partially catalytic wall correction will be applied to Eq. (9) in the pertinent flight regime.

The heating of the wing leading edge will be calculated using finite-length, swept-cylinder theory[14] as previously applied in Ref. 15. Since the shock-layer temperatures along most of the leading edge are too low to cause a significant amount of dissociation, finite-rate wall catalysis need not be considered. However, the leading-edge heating rate can be increased when boundary-layer transition to turbulence occurs, as in the case for the 5-km/s entry. (Boundary-layer transition data for air are used based on Refs. 16 and 17. The data were correlated as a function of boundary-layer edge Reynolds number and Mach number.) For turbulent boundary-layer heating, the expressions previously derived for air, and listed and applied in Ref. 15, are used. The equations of Ref. 15 were based on boundary-layer edge conditions, but correlated in terms of free-stream flight conditions and local

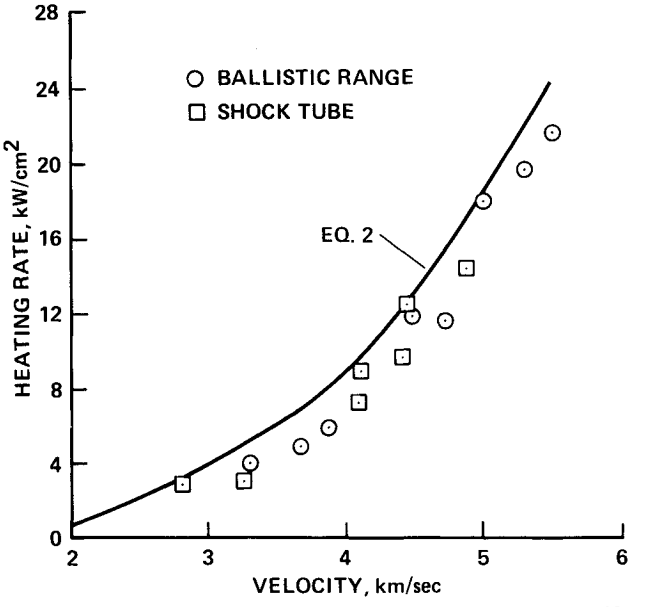

Fig. 1 Hemispherical stagnation-point heating rates in carbon dioxide, catalytic wall.

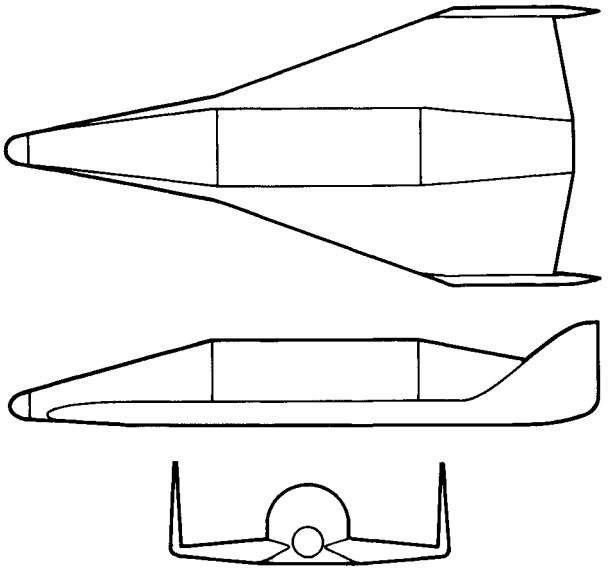

Fig. 2 Proposed vehicle configuration.

surface slopes. All heating calculations will be made assuming that the inviscid shock-layer flow is in equilibrium.

Results

The vehicle's high-speed aerodynamic characteristics in a predominantly CO_2 atmosphere will be presented first. The aerodynamics are calculated for flight conditions representative of both a high-altitude gliding trajectory and conditions experienced near the bottom of skips occurring during the 5-km/s entry. A range of entry angles is considered for the two types of trajectories, and the lateral distances covered are calculated. The heating at the stagnation point, and at a representative point on the wing leading edge, will be shown. Total heat inputs at the two body locations will be presented as a function of entry conditions. Where applicable, limiting heating rates are shown, assuming that a nonreusable, radiatively cooled heat shield is used. The resulting limiting equilibrium wall temperature is about 2100 K (corresponding to a heating rate of about 90 W/cm^2) for a conservative surface emissivity value of 0.8, which is used throughout the study.

Aerodynamic Performance

The vehicle's lift and drag are calculated at selected points in several trajectories with differing flow conditions. The 5-km/s entries that exhibit large-amplitude skipping motions encounter turbulent boundary-layer flow near the bottom of the skips. The 3.5-km/s entry trajectories have primarily laminar boundary-layer flows. The proposed vehicle's configuration is shown in Fig. 2. The nose radius is 30 cm and the wing has 70 deg of leading-edge sweep. A symmetric airfoil with a 6% thickness-to-chord ratio and with twice the leading-edge radius of the NACA 0006 section has been assumed. The larger leading-edge radius was selected to observe heating limits.

Three views of the proposed vehicle are shown in Fig. 2. The total length is about 10 m and the wingspan is 4.5 m. The vertical stabilizers are mounted on the wingtips to provide lateral stability and control at high angles of attack. An example of the vehicle's hypersonic aerodynamic characteristics is shown in Fig. 3. The maximum L/D is about 2.4 at angles of attack between 15 and 16 deg. The drag values shown in Fig. 3 are for an untrimmed vehicle flying at Mach 14 and having a local Reynolds number, based on mean aerodynamic chord, of 9×10^6. These flight conditions are experienced near the bottom of a high-speed skip, where the drag and heating are high since part of the vehicle's lifting surface has a turbulent boundary layer. After accounting for

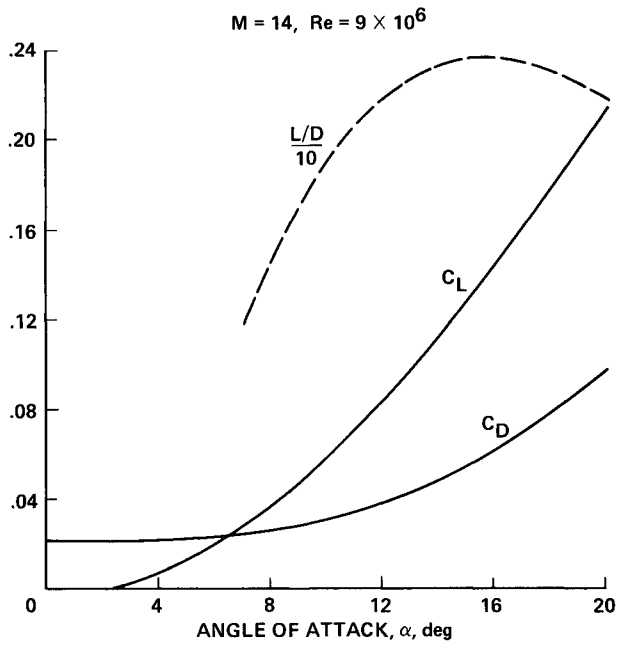

Fig. 3 Aerodynamic properties of vehicle.

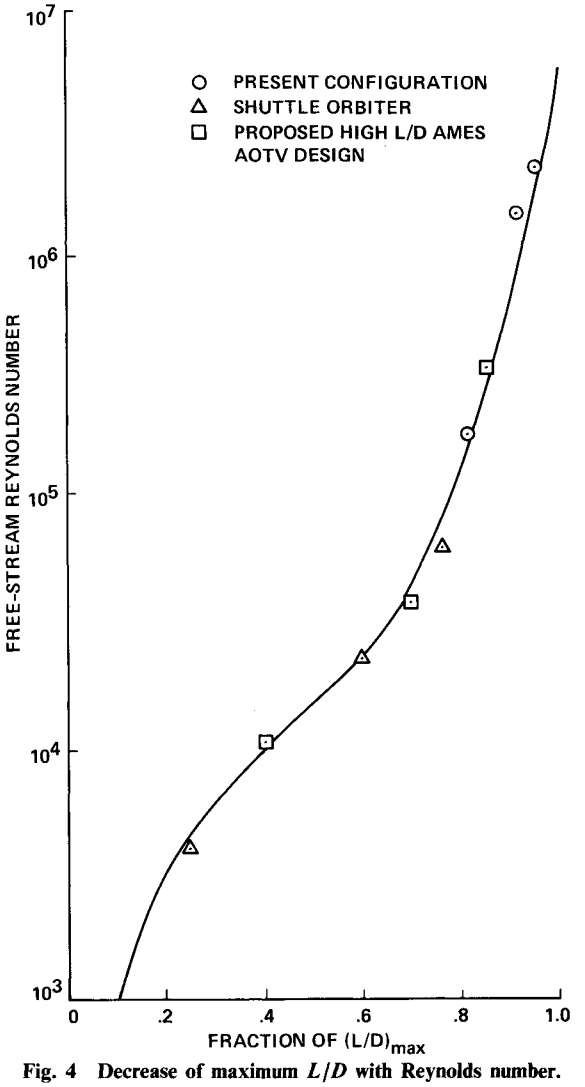

Fig. 4 Decrease of maximum L/D with Reynolds number.

trim drag (approximately), a conservative maximum L/D of 2.3 was used for all trajectory calculations. The peak L/D was varied with Reynolds number, however, to account for the

increased (laminar) skin friction experienced at high altitudes. The variation of peak L/D shown in Fig. 4 was based on calculated values for the present vehicle, the Shuttle orbiter, and a proposed, truncated, bent biconic high-L/D AOTV configuration.[18]

Entry Trajectories

Vehicles flying skipping trajectories, or maneuvering, can lose altitude rapidly in the tenuous Martian atmosphere. Therefore, care must be taken to prevent close approaches to the ground at high speeds to avoid collisions with mountains. The vehicle's descent rate can be controlled by stipulating a low wing loading and by using a maneuvering algorithm,[10] which maximizes the altitude at the conclusion of a gliding turn.

The variation of L/D with speed that is used during both longitudinal and maneuvering flight is shown in Fig. 5. At the parabolic entry velocity of 5 km/s, the L/D has to be modulated to ensure atmospheric capture during a single pass. Therefore, negative lift is required initially. The same L/D modulation is also applied to a lateral maneuvering trajectory in an effort to reduce the deceleration loads encountered during parabolic speed entry. Since the longest lateral ranges are reached by flying at a maximum L/D at the inception of the turn, the total deceleration loads can become substantial at parabolic entry speed, as will be shown.

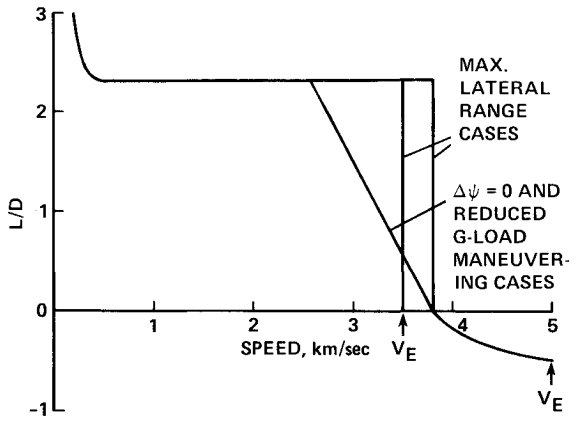

Fig. 5 Variation of L/D with flight speed.

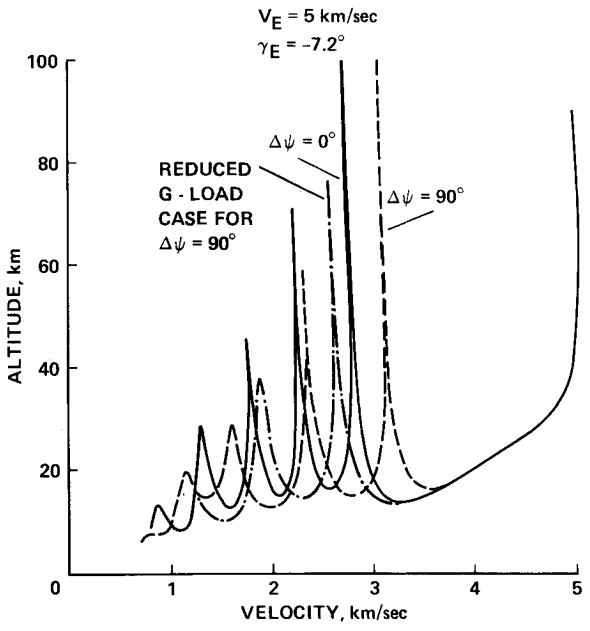

Fig. 6a Entry trajectories from highly elliptical Mars orbit.

Using the preceding control laws and an m/C_DA of 2000 kg/m^2, which is valid when the vehicle flies near its maximum L/D, three trajectories were computed and are illustrated in Fig. 6a. The entries occur at 5 km/s and at a flight-path angle of -7.2 deg at 90 km, or close to the minimum angle required for atmospheric capture. The cases labeled $\Delta\psi = 90$ deg are for lateral turning maneuvers begun at a speed of 3800 m/s. A constant bank angle of 53 deg is used until the turn is completed. The third trajectory, labeled $\Delta\psi = 0$, is a maximum longitudinal-range flight-path and is shown primarily for comparison. Note that all three trajectories exhibit large-amplitude skipping motion, but do not descend below a 13-km altitude at high speeds (except for the reduced g-load flight path, which reaches nearly 10 km).

Two gliding trajectories are illustrated in Fig. 6b. The entries occur at the circular speed of 3.5 km/s and at a flight-path angle of -1 deg at 90-km altitude. The initial period after entry, during which the vehicle accelerates slightly, is flown at zero lift to reduce the heating pulse length. The maximum lateral range turn is begun after the vehicle has decelerated to 3500 m/s. The bank angle is held constant at 47 deg until the turn is completed. After completing the turn, the vertical lift component increases as the vehicle is rolled from 47 deg back to zero, causing a modest skip.

The peak total deceleration loads experienced by the vehicle are shown in Fig. 7 for both entry velocities. The entry-angle range considered for the 5-km/s cases is small, since a 10-km altitude limit is exceeded at steeper angles than those shown and the loads increase rapidly. The lower g-load trajectory approaches within 5 km of the surface for a -7.3 deg entry angle; thus the vehicle has a very narrow flight corridor of less than 0.2 deg. At -7.2 deg, a 40% deceleration load reduction is realized; however, the load is still over 3 Earth g. In comparison, the circular-speed entries are much more benign. The peak decelerations, ranging from 0.67–0.9 Earth g, make these shallow gliding trajectories ideal for manned vehicles whose crews may have been physically weakened by the long voyage to Mars.

Heating and Lateral Ranges

For nonreusable, radiatively cooled, heat-shield materials, the limiting surface temperature is in the vicinity of 2100–

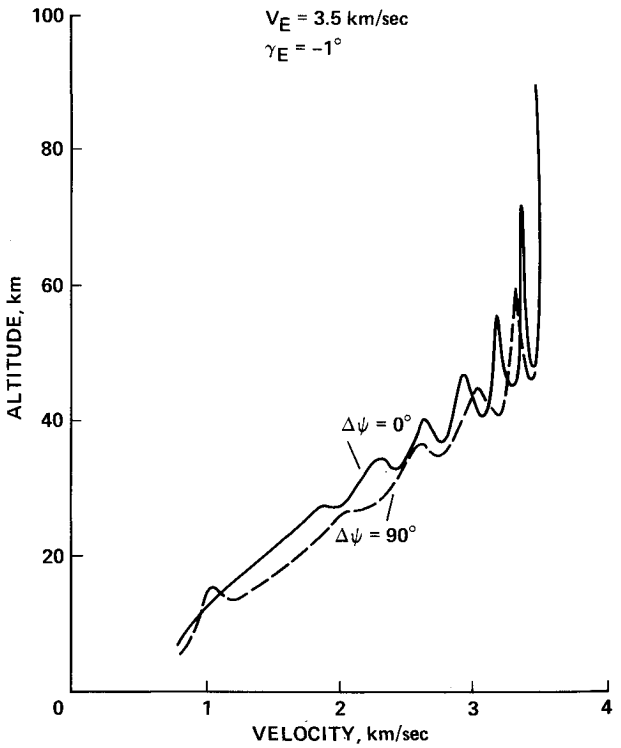

Fig. 6b Entry trajectories from low Mars orbit.

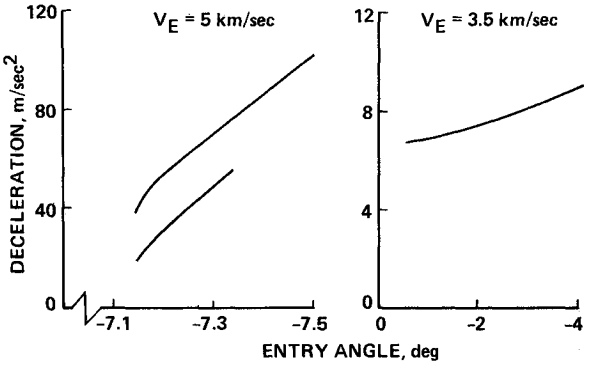

Fig. 7 Peak total deceleration loads during maximum lateral range entries.

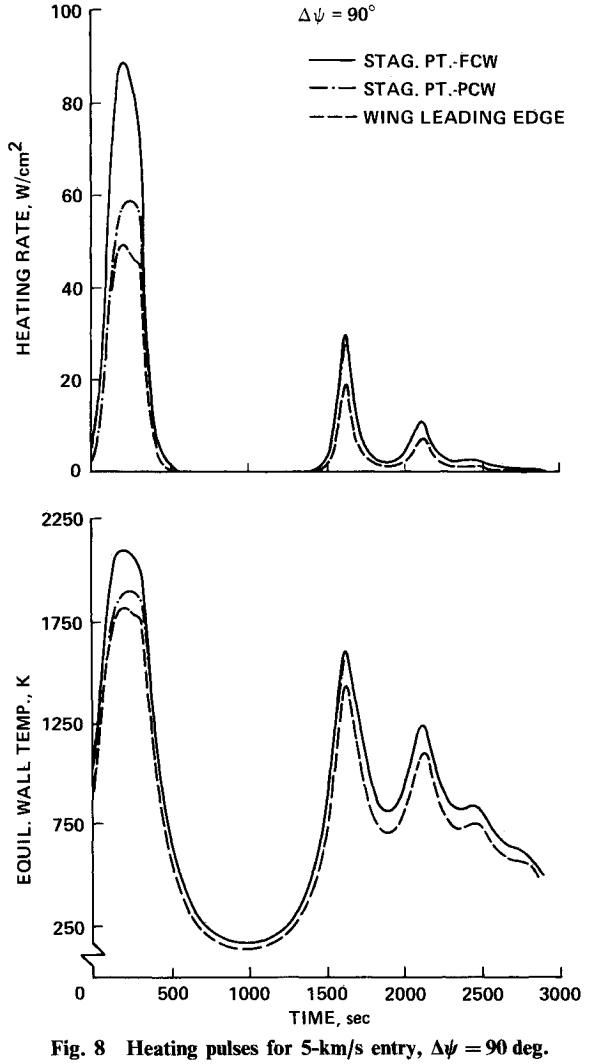

Fig. 8 Heating pulses for 5-km/s entry, $\Delta\psi = 90$ deg.

2200 K, corresponding to a heating rate of about 100 W/cm^2. (A surface emissivity of 0.8 has been assumed and will be used in all subsequent calculations.)

The highest heating rates on the vehicle will occur at the nose stagnation point and along the wing leading edge. The heating will be evaluated at the vehicle's stagnation point and at a representative point located 2 m along the wing leading edge where the radius is 6 cm. The stagnation-point heating rates will be shown (for a 30-cm nose radius) for both the conservative, fully catalytic, wall (FCW) and for the case which includes the estimated effect due to a partially catalytic wall (PCW). In addition, the corresponding equilibrium wall temperatures will be presented.

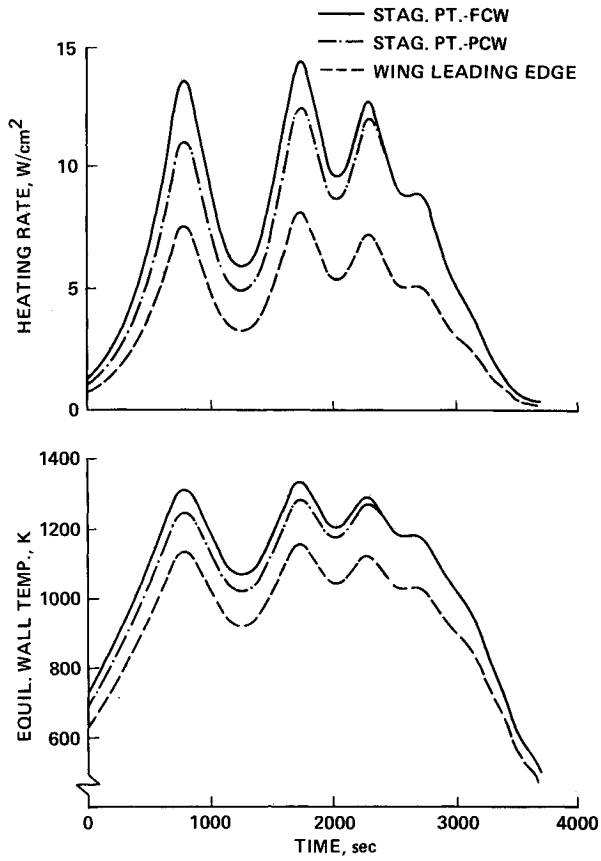

Fig. 9 Heating pulses for 3.5-km/s entry, $\Delta\psi = 90$ deg.

The heating and temperature variations with time are shown in Fig. 8 for the maneuvering entry at 5 km/s. Since the turn is initiated at a flight velocity of 3800 m/s, or about 300 s after entry, the maximum heating rates occur prior to this time. Near the bottom of each skip, the stagnation point experiences peak rates of about 90, 30, and 11 W/cm^2, resulting in wall temperatures of about 2100, 1600, and 1250 K, respectively. The heating at the leading-edge point is between one-half and two-thirds of the peak stagnation-point value. Note that despite the high heating rates that characterize skipping flight paths, the vehicle spends much time at very high altitudes where heating is negligible. During the high-altitude coast phases, the vehicle can radiate much of the previously absorbed heat to space.

The heating during gliding entry at 3.5 km/s from low Mars orbit is much lower for the 5-km/s entries, but the duration of the heating period is longer. The fluctuations in the heating rates results from the altitude oscillations that occur during the high-speed portion of the trajectory (see Fig. 6b). The extreme length of the heating pulse is due to flying a maximum L/D, long-lateral-range glide trajectory. For most trajectories, the vehicle would fly at a much lower L/D and at a high angle of attack, as is done with the Shuttle orbiter. Although the heating rates increase with angle of attack, the pulse is shortened because flight time is proportional to the L/D (Ref. 2). The peak stagnation-point heating rates range from 13.6 W/cm^2 to 11 W/cm^2 for the fully and partially catalytic walls, respectively (Fig. 9). The resultant wall temperatures are near 1300 K. The wing leading-edge heating rate peaks at 7.5 W/cm^2. However, the long flight times required to achieve large cross ranges will produce large total heat loads.

The weights of the vehicle's thermal protection system are approximately proportional to the total heat loads. Furthermore, the total heat input is proportional to the length of the heating pulse which decreases with increasing entry angle. In Fig. 10, the heat loads are shown for fully and partially

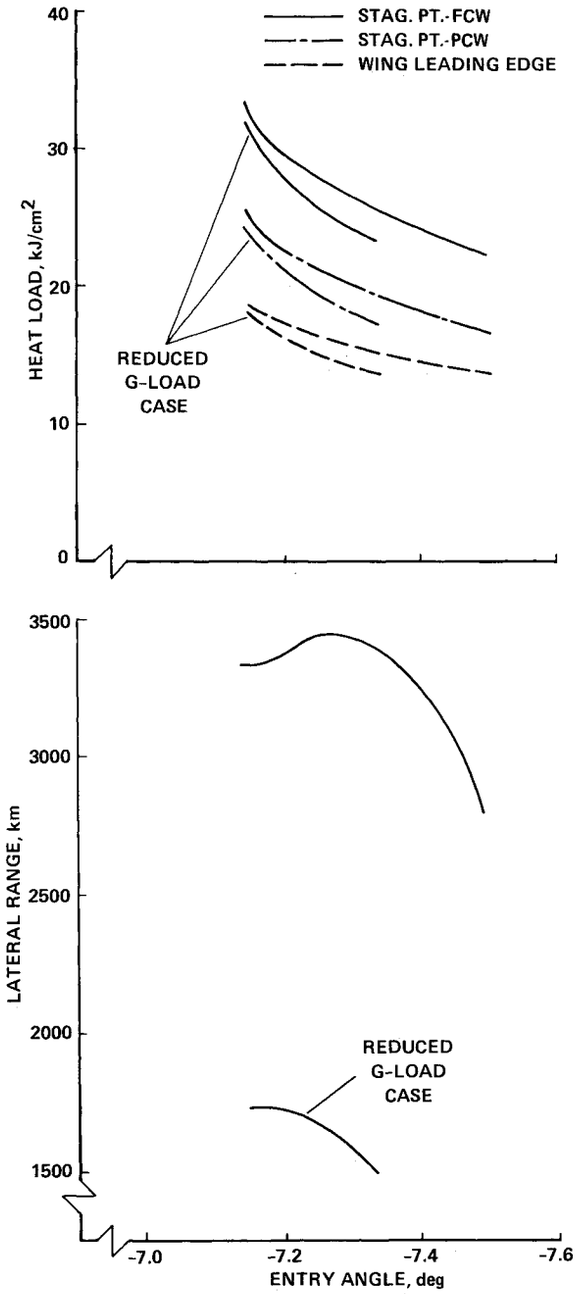

Fig. 10 Variation of total heat loads and lateral range with entry angle ($V_E = 5$ km/s).

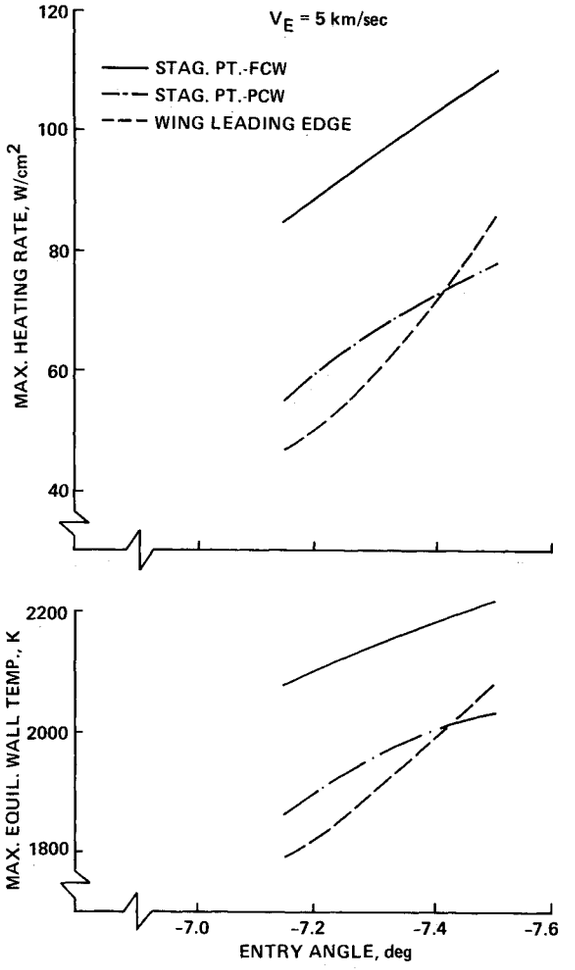

Fig. 11 Variation of maximum heating rate with entry angle.

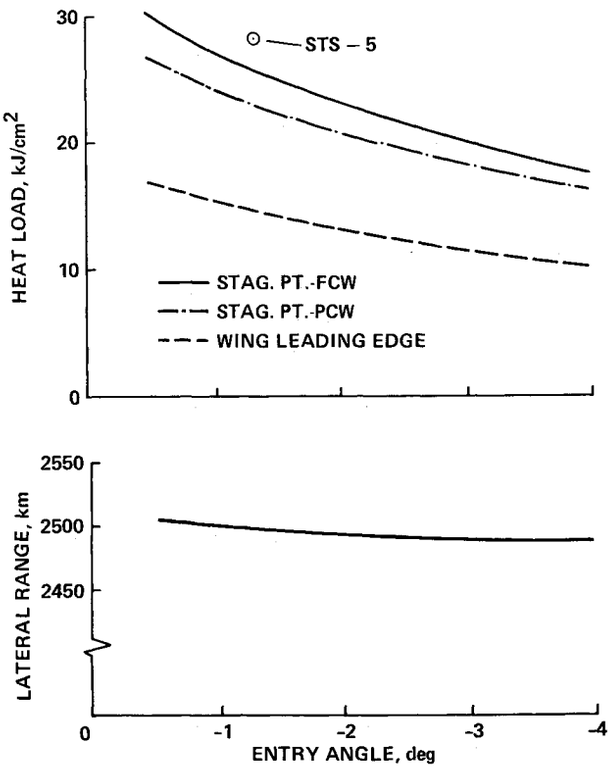

Fig. 12 Variation of total heat loads and lateral range with entry angle ($V_E = 3.5$ km/s).

catalytic surfaces at the stagnation point and on the wing leading edge. For the 5-km/s entries shown in Fig. 10, the heat loads decrease by approximately 30% with entry angle. The maximum lateral range is about 3400 km, but decreases to 2800 km at an entry angle of −7.5 deg. It is also apparent from Fig. 10 that using lift modulation to reduce the amplitudes of the skips to decrease the deceleration results in a 50% reduction in lateral range. The greatly increased guidance and control complexity and the much shorter cross range appear to be an excessively steep price for a moderate reduction in deceleration.

Since it is most efficient to cool the vehicle radiatively, maximum surface temperature limits must be observed. The peak heating rates and corresponding equilibrium wall temperatures for the parabolic speed entries are shown in Fig. 11. (The peak heating rates occur near the bottom of the first skip.[2]) The importance of using a surface material at the nose which is at least partially catalytic is evident if the 2100 K

temperature limit is to be observed. (The alternative is to increase the nose radius substantially, which would reduce the L/D.) The wing leading edge has a transitional, or turbulent, boundary layer which increases the peak heating. The very narrow range of acceptable entry angles is again evident for the 5-km/s entry cases.

For the 3.5-km/s entries, the peak heating rates and the equilibrium wall temperatures are moderate (see Fig. 9). However, because the flight times are longer for gliding trajectories, the total heat loads (Fig. 12) can exceed the value for the higher-speed entries. (The stagnation-point value for Shuttle flight 5 is also shown for comparison.) However, by increasing the entry angle from -1 deg to -4 deg, for example, the total heat loads can be reduced by about 35%. The accompanying decrease in the lateral range is negligible (see Fig. 12) when optimum bank angles are used.

Concluding Remarks

Atmospheric entries from highly elliptical Martian orbits at a speed of 5 km/s are much more difficult than entries from a low-altitude, circular orbit at a speed of 3.5 km/s. The higher-speed entries have much more stringent guidance requirements. (The acceptable entry flight path angle range is less than 0.5 deg if heating rates are limited so that the surface can be radiatively cooled.) In contrast, the lower-speed entries permit flight-path angle variations of at least 3 deg. A conservative maximum L/D of 2.3 was used for all of the trajectory calculations. The maximum achievable lateral ranges were 3400 km for the 5-km/s entries and 2500 km for the 3.5-km/s entries, permitting a wide choice of landing sites. However, the peak decelerations were an order of magnitude higher for the 5-km/s entries than for the 3.5-km/s entries. Efforts to moderate the altitude excursions and, therefore, the deceleration for the higher-speed entry by lift modulation achieved a 40% g-load reduction, but at the expense of a 50% decrease in the lateral range.

Radiative cooling of the vehicle appears feasible for both entry speeds. However, the vehicle entering at 3.5 km/s along a gliding trajectory encounters a much more benign atmospheric environment. The heat loads for both entry speeds are roughly comparable, since the glider experiences a longer heating pulse. However, the glider's peak equilibrium wall temperatures are about 700 K lower for the nominal entries. Also, the glider's peak deceleration is only about 0.7 Earth g. Therefore, the shallow flight path is well-suited to manned vehicles whose crews may have been physically weakened during the long voyage to Mars. However, the benign environment encountered during entry from a low satellite orbit is achieved at some expense. The vehicle's kinetic energy, using either propulsive or atmospheric braking, must be reduced to half the value for a highly elliptical orbit.

References

[1]Seiff, A. and Kirk, D. B., "Structure of the Atmosphere of Mars in Summer at Mid-Latitudes," *Journal of Geophysical Research*, Vol. 82, Sept. 1977, pp. 4364–4378.

[2]Tauber, M. E. and Yang, L., "Performance Comparisons of Maneuvering Vehicles Returning from Orbit," AIAA Paper 87-2490, Aug. 1987.

[3]Russell, W. R. (ed.), *Space Shuttle Transportation System-Operational Aerodynamic Data Book*, Rockwell International, Downey, CA, STS85-0118, Sept. 1985.

[4]Roberts, C., "PIECES and CEN User's Guides," Tech Note 13, Sterling Federal Systems, Inc., Palo Alto, CA, 1988.

[5]Bailey, H. F., "Equilibrium Thermodynamic Properties of Carbon Dioxide," NASA SP-3014, 1965.

[6]Eckert, E. R. G., "Survey on Heat Transfer at High Speeds," Univ. of Minnesota, Aeronautical Research Lab., Rept. 189, Dec. 1961.

[7]Lee, J. and Bobbitt, P., "Transport Properties at High Temperatures of CO_2–N_2–O_2–Ar Gas Mixtures for Planetary Entry Applications," NASA TND-5476, Nov. 1969.

[8]Hoerner, S. F., *Fluid Dynamic Drag*, S. F. Hoerner, Midland Park, New Jersey, 1958, Chap. 8.

[9]Vinh, N. X., Busemann, A., and Culp, R., *Hypersonic and Planetary Flight Mechanics*, Univ. of Michigan Press, Ann Arbor, Michigan, 1980.

[10]Tauber, M. E., "Hypervelocity Gliding Maneuvers," *Journal of Aircraft*, Aug. 1987, pp. 572–574.

[11]Woodward, H. T., "Predictions of Shock-Layer Radiation from Molecular Band Systems in Proposed Planetary Atmospheres," NASA TN D-3850, Feb. 1967.

[12]Marvin, J. G. and Deiwert, G. S., "Convective Heat Transfer in Planetary Gases," NASA TR R-224, July 1965.

[13]Yee, L., Bailey, H. E., and Woodward, H. T., "Ballistic Range Measurements of Stagnation-Point Heat Transfer in Air and in Carbon Dioxide at Velocities Up to 18,000 Feet per Second," NASA TN D-777, March 1961.

[14]Rubesin, M. W., "The Effect of Boundary-Layer Growth Along Swept-Wing Leading Edges," Vidya Corp., Palo Alto, CA, Rept. 4, 1958.

[15]Tauber, M. E., Menees, G. P., and Adelman, H., "Aerothermodynamics of Transatmospheric Vehicles," *Journal of Aircraft*, Vol. 24, Sept. 1987, pp. 594–602.

[16]Morkovin, M. V., "Critical Evaluation of Transition from Laminar to Turbulent Shear Layers with Emphasis on Hypersonically Traveling Bodies," Air Force Flight Dynamics Laboratory, Wright-Patterson AFB, OH, AFFDL-TR-68-149, March, 1969.

[17]Throckmorton, D. A., "Benchmark Determination of Shuttle Orbiter Entry Aerodynamic Heat-Transfer Data," *Journal of Spacecraft and Rockets*, Vol. 20, May–June 1983, pp. 219–224.

[18]Davies, C. B. and Park, C., "Optimum Configuration of High-Lift Aeromaneuvering Orbital Transfer Vehicles in Viscous Flow," AIAA Paper 85-1059, June 1985.